# 6

# Finite Element Modeling of Ventricular Mechanics

**Julius M. Guccione**[1]
**Andrew D. McCulloch**[1]

ABSTRACT Computing the distributions of stress and strain in a body with the complex geometry, boundary conditions, and material properties of the heart is a difficult yet worthwhile endeavor. The most promising method for obtaining numerical solutions to this problem is the finite element method. In this chapter, we review the use of finite element analysis for modeling ventricular mechanics. And we conclude by presenting a new axisymmetric finite element model of the passive left ventricle with a realistic geometry and fibrous architecture, physiological boundary conditions, and a three-dimensional constitutive equation.

## 6.1 Introduction

The distributions of stress in the ventricles of the heart are determined by (1) the three-dimensional geometry and fibrous architecture of the ventricular walls, (2) the boundary conditions imposed by the ventricular cavity and pericardial pressures and structures like the fibrous valve ring skeleton at the base of the ventricles, and (3) the three-dimensional mechanical properties of the myofibers and their collagen interconnections in the relaxed and actively contracting states. Many of these determining factors have been quantified in experimental studies, some of which are described in detail in this book.

For example, Streeter and Hanna [72,73] and Nielsen and coworkers [56] have made detailed studies of the three-dimensional geometry and myocardial fiber architecture of the ventricles of the dog heart. Measurements of left and right ventricular pressures in patients are quite routine. And extensive data have been collected on the passive and active uniaxial material properties of isolated papillary muscles and trabeculae from various mammalian species [64,74]. Although fully triaxial material testing still presents significant technical difficulties, biaxial stress-strain testing of excised two-

[1]Department of Applied Mechanics and Engineering Sciences (Bioengineering), University of California, San Diego, La Jolla, California 92093

L. Glass et al. (eds.), *Theory of Heart*

dimensional sheets of passive canine myocardium [14,91], epicardium [30], and pericardium [43] has been performed.

To formulate a mathematical model for predicting the distributions of wall stress in such a complex and constantly changing mechanical system is clearly very difficult, but there are important reasons to attempt this. An accurate model of the mechanics of the ventricular myocardium would provide a sound basis for interpreting the complex regional changes in cardiac function that occur in pathological conditions, such as ischemic heart disease [44,75], in terms of changes in the local properties of the tissue. Knowledge of the stress distributions in the intact myocardium would also provide valuable insight into normal ventricular function since regional coronary blood flow [34], myocardial oxygen consumption [68], hypertrophy, and remodeling [2,19] are all influenced by ventricular wall stress [90].

To keep the problem mathematically tractable, many workers have developed models of left ventricular mechanics using simple geometric approximations such as thin-walled spheres [88], thin-walled ellipsoids [16,67,86], thick-walled ellipsoids [8,21,51,52,80,87], thick-walled spheres [1,15,53,54, 69,83], thick-walled cylinders [4–6,11,17,24,34,57,58,76,79], solids of revolution [35], and noncircular cylinders [39]. However, the analyses made by these models also make other simplifying assumptions about the material behavior of the heart muscle and the governing equations of motion.

All thin-walled membrane models and even some thick-walled models [35,39] only predict the average stress across the wall thickness because they are based on a global force balance (the "Law of Laplace"); they are not based on knowledge of material properties. In order to predict transmural stress distributions using a thick-walled ellipsoidal model, either the inappropriate linear (infinitesimal strain) theory of elasticity has been assumed [21,51,52,87] or the wall has been represented by nested layers of uncoupled membranes [8,80], which neglects the tethering between adjacent layers of muscle fibers [10,66]. Some thick-walled spherical models have employed the nonlinear finite deformation theory of elasticity, which is more appropriate since experimental measurements of ventricular deformations have shown that myocardial stretches during normal diastolic filling and shortening strains during systole may be 20% or greater. However, material isotropy [15,53,54,83] or, at best, transverse isotropy with respect to the radial direction [1,69] was needed for the solution of these models so that the spherical symmetry was preserved upon inflation or ejection.

Most of the thick-walled cylindrical models, whether using concentric shells [4–6,34], finite elasticity [17,76,79], or linear elasticity [11,57,58], have incorporated a fiber-in-fluid material representation of the myocardium to study the effect of the transmural variation in muscle fiber orientation on the profiles of diastolic or systolic stress in the left ventricular wall. The fluid-fiber assumption that tension can only be borne in the muscle-fiber direction is not, however, supported by biaxial material tests of passive myocardium [14,91], which have shown that ventricular muscle can bear

significant loads acting in directions transverse to the fibers. Moreover, in the intact beating heart, it has been found by Waldman and coworkers [84,85] that the direction of greatest muscle shortening does not necessarily coincide with the muscle-fiber direction, especially near the endocardium where the major axis of shortening may actually be perpendicular to the fibers. Nevertheless, unlike many other models, some of the cylindrical fluid-fiber models have been able to demonstrate the ventricular torsion [4–6,11,57,58,76] that has long been observed (see Ingels and colleagues, [33]). Interestingly, their predicted stress distributions sometimes differed significantly from those cylindrical models that did not have the freedom to twist [17,34,80].

The stresses predicted by models of ventricular mechanics cannot be directly verified because the direct measurement of local forces in the intact heart wall has not been entirely successful [29,90]. However, experimental measurements of myocardial strains have been used for model validation. Arts and coworkers [5] compared the deformations predicted by their cylindrical model of the ejecting left ventricle with systolic strains measured on the epicardium of open-chest canines using a triangular arrangement of inductance gauges. We [24] have used experimental measurements of myocardial strains to validate a thick-walled cylindrical model of the passive left ventricle that employed finite deformation theory and a three-dimensional constitutive equation referred to a system of fiber coordinates. By optimizing material parameters, the model was able to reproduce the circumferential, longitudinal, and torsional epicardial strains that had been measured in the isolated arrested dog heart, as described by McCulloch and Omens in Chapter 5 of this book.

However, cylindrical models are probably confined at best to describing the mechanics of a narrow equatorial cross-section of the left ventricular wall. Such simple models are not suitable for analyzing the nonhomogeneous effects of three-dimensional variations in the geometry, fiber orientations, and mechanical properties of the heart. Nor are factors like diastolic and systolic ventricular interactions or the motion constraints imposed by the pericardium, valve rings, and papillary muscles able to be included realistically in a cylindrical model.

Nielsen and colleagues [56] needed a three-dimensional mathematical model with a complex variation in radius and wall thickness to obtain an accurate approximation to their measurements of ventricular geometry. They also measured the distributions of muscle-fiber orientation in the canine heart and found that transmural fiber angle profiles vary significantly between the two ventricles as well as between the free walls and the interventricular septum.

Another source of heterogeneity in ventricular mechanics is the partly asynchronous activation of the myocardium, which is first activated near the apical endocardium where the wave of depolarization travels rapidly along the Purkinje fiber network toward the base and more slowly to the

epicardium through muscle cell conduction with a wave-speed along the muscle fibers that is roughly two to three times that in directions transverse to the fibers [32]. In myocardial infarction, a large portion of the left ventricular wall may become stiff and scarred with no active function. Increased diastolic filling of one ventricle impedes filling of the other [18]. Direct interaction between right and left ventricles during systole has been shown to affect ventricular contraction and relaxation in the intact heart under normal conditions [70]. Diastolic ventricular interaction can be affected by the presence of the pericardium [22]. Severing the chordae tendineae of the mitral valve produces systolic bulging in the region of the papillary muscle insertions [26]. Together, these factors contribute to the regional variations in local ventricular deformations that have been observed in experimental preparations and clinical studies.

For example, passive epicardial stretches measured in the isolated arrested canine heart [48] and systolic shortening measured on the epicardium in humans [41] and at the midwall in dogs [46] were all found to increase in magnitude from the base to the apex of the left ventricular free wall. A similar longitudinal variation in shortening was also observed on the epicardium of the canine right ventricle by Meier and colleagues [49]. Lew and LeWinter [45] measured significantly greater systolic midwall shortening on the anterior free wall than on the posterior free wall of the canine left ventricle. And Kong and colleagues [41] found that systolic shortening in patients was greater on the left ventricular free wall than in the interventricular septum.

## 6.2 The Finite Element Method

To solve the governing equations of equilibrium for a body with such a complex geometry, boundary conditions, and material properties, computational techniques are required. The most versatile method is the finite element method in which the dependent variables are discretized by piecewise polynomial approximations over finite subdomains (elements) and expressed in terms of parameter values at interelement connection points (nodes).

As early as 1906, researchers first began suggesting the solution of continuum mechanics problems by modeling the body with a lattice of elastic bars and employing frame analysis methods (see Cook, [13]). In 1941, Courant recognized piecewise polynomial interpolation over triangular subregions as a Rayleigh-Ritz solution of a variational problem. Since there were no computers at the time, neither approach was practical and Courant's work was largely forgotten until engineers had independently developed it. By 1953, structural engineers were solving matrix stiffness equations with digital computers. The widespread use of finite element methods in engineering began with the classic papers by Turner and colleagues [78] Argyris and

Kelsey [3]. The name "finite element" was coined in 1960, and the method began to be recognized as mathematically rigorous by 1963.

Many finite element models of ventricular mechanics have been proposed, although most of them did not include the nonlinear kinematic terms associated with large deformations because iterative solution to the nonlinear governing equations at each load step is required. The importance of adopting nonlinear finite deformation theory for the analysis was demonstrated by Janz and colleagues [38]. However, their model along with a few subsequent finite element models based on finite deformation theory [25,40,92] and most of the linear models [9,20,23,27,36,55,61,62,65] treated the myocardium as an isotropic material. The effect of the ventricular muscle-fiber distribution has been modeled with finite elements that possess material anisotropy with respect to a continuously varying fiber axis [7,28,31] or more commonly by using a number of concentric elements, each with a constant fiber direction [12,60,63,89]. The incompressibility of the heart muscle, which is composed mostly of water, was very often accounted for incorrectly by assuming that the myocardium has a Poisson ratio close to 0.5 [12,20,27,36,37,61,63,82,89]. More correctly, in the context of finite deformations, the hydrostatic pressure—an extra dependent variable arising from the kinematic incompressibility constraint—is introduced as a Lagrange multiplier in the strain energy function[2] [7,25,28,31,81]. Although a few models consider muscle activation and contraction [7,25,63], the rest have been concerned with the accurate prediction of end-diastolic stresses and sarcomere length distributions, a prerequisite for a realistic model of active ventricular contraction.

Whereas a considerable body of information is available on the heterogeneity of wall motions in the beating heart, regional strain measurements suitable for validating models of the passive left ventricle have only recently become available [48]. Only the finite element model predictions of McCulloch [47] and Hunter and colleagues [31] have been tested with experimental strain data. However, these comparisons were made at just one location on the epicardial surface and the rather poor agreement was largely attributable to the somewhat arbitrary myocardial stress-strain relation that these investigators chose and their simplified geometries, which were each modeled with only one finite element. In this chapter, we employ the finite element method of Hunter, McCulloch and coworkers [31], but we adopt a new constitutive equation and we extend the model to a

[2]It should be noted that although the "hydrostatic pressure" does have units of stress and is added to the diagonal components of the stress tensor in the manner of a pressure, it does not itself coincide either with the mean stress at a point in the myocardium (the "intramyocardial pressure") or with the boundary pressures loading the ventricular wall. It is further unsuited to direct physical interpretation since it may not even be zero in the stress-free body.

more realistic axisymmetric geometry with more physiological boundary conditions.

## 6.3 An Axisymmetric Finite Element Model of the Passive Left Ventricle

Our finite element method was specifically developed for continuum analysis of the heart [31,47]. Hence, the approach includes several special features uncommon to conventional finite element methods. The Galerkin finite element equations for three-dimensional finite elasticity were derived in general tensor form and then specialized for four alternative reference coordinate systems: rectangular Cartesian, cylindrical polar, spherical polar, and prolate spheroidal. Therefore, using conforming isoparametric elements with tensor-product basis functions for each of the geometric coordinates, only one axisymmetric element with four global nodes was needed to model each of the cylindrical, spherical, and prolate spheroidal geometries illustrated in Figure 6.1. By formulating the governing equations in a coordinate system that simplifies the geometric description of the deforming body, the greater algebraic complexity is more than compensated by a significant reduction in the number of degrees of freedom required for the finite element discretization. The resulting nonlinear system of global equilibrium equations are solved, subject to appropriate boundary conditions, for the nodal displacement and hydrostatic pressure parameters using a quasi-Newton iteration scheme.

For incompressible bodies, the kinematics of the deformation are constrained by the condition that the volume of any arbitrarily small part of the wall must remain constant. For most finite element schemes, this condition can be satisfied only in the average sense for the entire finite element. However, significant improvement in the finite element stress and strain solutions was obtained using a new "isochoric" element interpolation method with which—in geometrically simple bodies such as cylinders or spheres—the kinematic incompressibility constraint was satisfied exactly throughout the element. In these isochoric elements, rather than interpolate the radial coordinate ($r$ in a polar system), we interpolate an appropriate function of $r$ that is proportional to the wall volume—that is, $r^2$ in the case of cylindrical elements, or $r^3$ in the case of spherical ones. In prolate spheroidal coordinates $(\lambda, \mu, \theta)$, the function is less intuitive ($d^3 \sinh^2 \lambda \cosh \lambda$, where $d$ is the focal length) but the idea is the same. For problems with more complex geometries the isochoric elements are no longer kinematically exact, but they still result in a considerable improvement in accuracy for incompressible finite deformations.

Since the dependent variables in the formulation of the model are the nodal displacements and the hydrostatic pressure variable that arises from

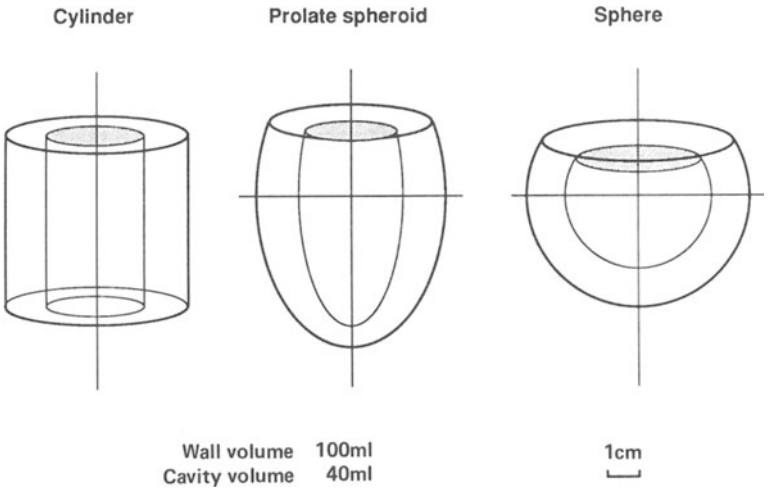


FIGURE 6.1. The cylindrical, prolate spheroidal, and spherical finite element models of the left ventricle used by Hunter et al. [31]. These geometries were each modeled exactly by a single axisymmetric finite element. All three geometric models had a wall volume of 100 ml and an undeformed cavity volume of 40 ml based on experimental measurements from the canine heart. (Reproduced from Hunter et al. [31], with permission from the ASME.)

the incompressibility condition, this finite element problem is a "mixed" formulation. With such formulations, a compatibility condition that relates the pressure and displacement approximating spaces must be satisfied to ensure that a given displacement field corresponds to a unique solution for the hydrostatic pressure [42]. In practice, this requires that for a linear nodal interpolation of the geometric parameters, such as in the elements shown in Figure 6.1, a single constant hydrostatic pressure parameter is all that can be permitted for each element to avoid numerical ill-conditioning. Since the incompressible deformation of thick-walled vessels results in a nonlinear transmural distribution of hydrostatic pressure, several finite elements each with a constant pressure are usually required through the wall thickness. However, because the ventricles of the heart are loaded by boundary pressures, it was possible to increase the hydrostatic pressure interpolation to a quadratic transmural variation by using the boundary pressures prescribed on the inner and outer surfaces of the element as additional constraints. This results in stress solutions that closely or exactly match the boundary stress field, and for simple axisymmetric problems to which closed-form solutions exist, the results obtained with a single finite element were found to be practically exact throughout the wall [47].

The material anisotropy of the heart muscle is defined by referring the element stress components to a system of embedded material coordinates, which is orthogonal in the undeformed state and has one axis aligned with the fiber direction. The fiber axis lies in the plane of the wall so that it is tangential to the boundary at the endocardium and the epicardium, but the in-plane fiber angle can change continuously through the element as defined by an appropriate nodal finite element interpolation. In the constitutive equation for stress, the myocardium is modeled as transversely isotropic with respect to the local fiber axis. These three-dimensional, curvilinear, isochoric finite elements with stress boundary constraints and embedded fiber fields meet the most important requirements for modeling passive ventricular mechanics. However, the stresses predicted by these finite elements will depend on the geometry, fiber angle distribution, material properties, displacement constraints, and loading assumed in the model.

In the study of Hunter and coworkers [31], the canine left ventricle was represented by the cylindrical, spheroidal, and prolate spheroidal finite elements shown in Figure 6.1, with a cubic variation of fiber angle across the wall from $-60°$ on the epicardium to $+60°$ on the endocardium. The myocardium was modeled both as an isotropic and as a transversely isotropic, homogeneous elastic material. All three geometric models were constrained from extending axially and rotating at the base. A uniform cavity pressure was applied to the endocardium while the epicardial pressure remained zero. For the isotropic material model, the material constants of an exponential stress-strain relation (strain energy function) were chosen to fit sarcomere length-tension measurements from isolated muscle preparations [74]. To examine the effects of transverse isotropy without altering the prop-

erties of the model material along the fiber direction, the uniaxial tensile stiffness in the transverse plane was scaled up by a constant factor chosen rather arbitrarily to be 16. The authors acknowledged that there was no firm foundation for this choice. It was based on the observation that the isotropic models were too compliant in that they significantly overestimated passive ventricular volumes at physiological pressure loads. Since the stress-strain behavior of the isotropic models had been fitted to accurate measurements of muscle sarcomere length-tension relations, the authors postulated that the additional muscle stiffness needed to produce a more physiological pressure-volume relation might be added in the transverse plane without necessarily changing the uniaxial properties of the model material in the fiber direction.

These models were evaluated by comparing predicted epicardial deformations with experimental measurements from the midanterior wall of the isolated potassium-arrested dog heart [48]. In this region, the observed principal angle of greatest stretch was consistently clockwise from circumferential, tending to increase with pressure to coincide closely with the epicardial fiber angle (mean, $-42 \pm 7°$) at high loads. This principal angle was also consistent with the torsional deformation of the ventricle that was observed. However, the principal stretches of the three isotropic models were aligned with the circumferential and longitudinal axes, so the principal angles were always zero and there was no torsion. Although the transversely isotropic models did twist upon inflation, the predicted epicardial extensions did not correspond closely with the experimental measurements. In the prolate spheroidal model, the epicardium twisted in the same direction as the experimental preparation at low pressures, but reversed direction as the load increased.

These workers had hypothesized that by making the passive myocardium most compliant in the fiber direction, the predicted epicardial extensions during filling would be greatest along this axis as they had observed experimentally. But they found that their anisotropic models were not highly sensitive to increases in the transverse stiffness, especially in the cylindrical model, which was prevented from extending longitudinally. However, in the analytical model subsequently proposed by Guccione and coworkers [24], we found that the amount a cylinder twists and extends upon inflation is indeed sensitive to the biaxial stiffness ratio and also to the fiber angle distribution. As described in Chapter 5, we obtained estimates for the parameters of a transversely isotropic material defined with an exponential strain-energy function by minimizing the differences between the experimental and model-predicted strains using a semi-inverse approach. Somewhat surprisingly, the optimal material was stiffest in the fiber direction, not the transverse direction. The fiber-to-transverse stiffness ratio[3]

[3]This stiffness ratio was defined as the stiffness in the fiber direction divided by

was 3.3. Here we extend the work of Hunter and coworkers [31] beyond the three simple test shapes to an axisymmetric model of the passive left ventricular free wall that incorporates the following form of the strain-energy function used by Guccione and colleagues [24]:

$$W = \frac{C}{2}(e^Q - 1) - \frac{1}{2}p(I_3 - 1) \tag{6.1}$$

where $C$ is a constant, $p$ is the hydrostatic pressure variable, $I_3$ is the third principal strain invariant, which is unity for an incompressible deformation, and

$$Q = b_1 E_{11}^2 + b_2(E_{22}^2 + E_{33}^2 + E_{23}^2 + E_{32}^2) + b_3(E_{12}^2 + E_{21}^2 + E_{13}^2 + E_{31}^2) \tag{6.2}$$

where $b_1$, $b_2$, and $b_3$ are material constants and $E_{RS}$ are Lagrangian strain components referred to the (undeformed) fiber coordinate system $\{X_R\}$, where $X_1$ is aligned with the muscle fibers, $X_2$ is the cross-fiber in-plane axis, and $X_3$ is the transmural coordinate. The material defined by Equations (6.1) and (6.2) possesses symmetry under the group of all rotations about the $X_1$-axis, and is therefore said to be "transversely isotropic" about $X_1$. The fiber angle used in the following models varied linearly from $\phi_i$ on the endocardium to $\phi_o$ at the epicardium, and the material constants in Equations (6.1) and (6.2) were $C = 0.88$ kPa, $b_1 = 18.5$, $b_2 = 3.58$, and $b_3 = 1.63$.

For comparison with the earlier results, we began with the one-element axisymmetric prolate spheroidal model as shown in Figure 6.2. The solid lines represent the unloaded reference state. The undeformed cavity volume was 40 ml and the volume of the ventricular myocardium was 100 ml, typical of the canine heart. The focus of the ellipsoidal surfaces was 3.75 cm and the basal plane was 30° from the equator as suggested by Streeter and Hanna [73]. At all longitudinal coordinates ($\mu$), the transmural fiber angle distribution was defined by $\phi_i = 65°$ and $\phi_o = -55°$.

We assumed that there is no stress in the passive ventricular wall when the filling pressure is zero. However, recently it has been shown that the unloaded left ventricle is not stress-free. Omens and Fung [59] have demonstrated that when a cross-sectional ring of the freshly excised potassium-arrested rat heart is cut radially, it springs open to form an arc, as described by McCulloch and Omens in the previous chapter. Although such experiments have not yet been reported for the canine heart, the analysis of Guccione and colleagues [24] showed that the effect of this opening angle on end-diastolic stresses was significant, although the estimated material properties were not particularly sensitive to this quantity. However, it is not yet clear how to incorporate residual stresses in an axisymmetric finite element model. Since the governing equations are nonlinear, the initial

---

the stiffness in the transverse plane that would be measured in a plane equibiaxial stretch of 1.2.

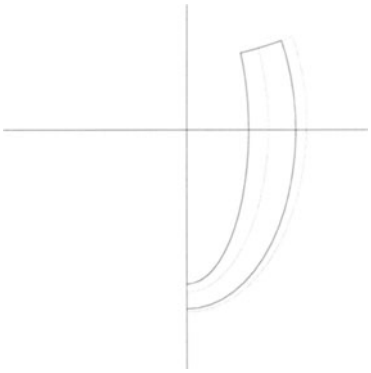

FIGURE 6.2. One-element prolate spheroidal model of the canine left ventricle. The unloaded reference state (solid lines) was bounded in the prolate spheroidal coordinate system by the surfaces defined by $\lambda = 0.43, \lambda = 0.72$, and $\mu = 120°$. Muscle-fiber angle varied linearly from 65° (endocardium) to −55° (epicardium) where zero corresponds to the circumferential direction and a positive angle is rotated counterclockwise. The dotted lines show the deformed profile for a ventricular pressure of 2 kPa (15 mm Hg).

stresses cannot be superposed in the solution. And if the residual stresses are added to the stresses in the constitutive equation, the resulting relation no longer satisfies the principal of material frame indifference. Therefore at this stage, the residual stress phenomenon is not included in our finite element models.

Using a single isochoric element, the deformed profile shown in dotted lines in Figure 6.2 was obtained for inflation to a ventricular pressure of 2.0 kPa (15 mm Hg). It shows that the deformation was greatest near the base and in the radial direction, and therefore circumferential stretch was dominant. This is shown by the dotted line in Figure 6.3, where the major principal stretch at the midanterior epicardium is plotted against the mutually perpendicular minor stretch for ventricular pressures up to 0.8 kPa. The results for the one-element model show that, in comparison with the experimental measurements, the epicardial strains were too nonuniform and the model deformed more like an inflated cylindrical tube (a vertical line) than a spherical balloon (a slope of one). Although the predicted principal angles of the major stretch were within one standard error of the experimental measurements at the lower loads (Figure 6.4, dotted line), the experimental means varied with load from −22° to −52°, whereas the predicted angles remained quite constant at −13° to −15°. Consequently, the one-element model did predict torsion in the same direction as observed experimentally at all loads; however, the amount was now exaggerated in the model (7.6° compared with 4.1° at the highest load).

To simulate the effects of the relatively stiff mitral valve ring on left ven-

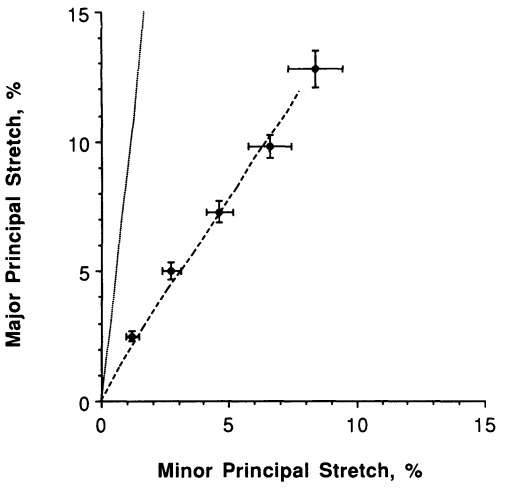


FIGURE 6.3. Major principal stretches at the midanterior epicardium plotted against the mutually perpendicular minor stretches at various left ventricular pressures. The experimental measurements (solid circles) of McCulloch et al. [48] are compared with the predictions of the one-element prolate spheroidal model (dotted line) and the 14-element prolate spheroidal model (dashed line). The error bars on the experimental measurements indicate one standard error of the mean. The five experimental points are for mean left ventricular pressures of approximately 0.2, 0.4, 0.7, 1.1, and 1.7 kPa.

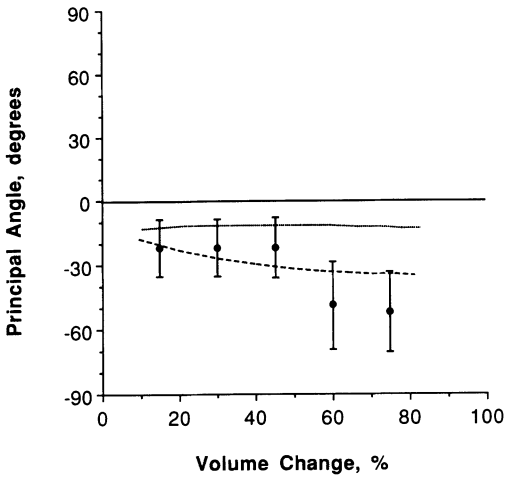


FIGURE 6.4. The principal angle of the major stretch on the midanterior epicardium plotted against left ventricular volume change. The experimental measurements (solid circles) of McCulloch et al. [48] at five left ventricular pressures are compared with the predictions of the one-element model (dotted line) and the 14-element model (dashed line). The error bars on the experimental measurements indicate one standard error of the mean.

tricular filling and make the model bulge more like a sphere, we constrained the prolate spheroidal mesh by preventing displacement of the epicardium at the base of the model. But to obtain a converged solution for this problem required considerably more degrees of freedom along the longitudinal direction than the one-element case. Therefore, the model was subdivided repeatedly into elements equally spaced along the longitudinal coordinate ($\mu$). However, even with 16 such elements, the convergence criteria for accurate stress solutions near the base and apex were not met. To reduce the required computation, an optimum mesh layout with a minimum number of nodes was sought. To determine which portions of the mesh required refinement or optimization, the differences between the strain energy densities at neighboring Gaussian quadrature integration points within each element and across each interelement boundary were computed. A large difference indicates departure from constant strain conditions and suggests the need for mesh refinement [50,77]. The positions of the element boundaries were adjusted until these strain energy density differences were less than 10% throughout the longitude. Thus, we found that only regions near the base and apex needed refining. By having several small elements at the base and apex and a few larger elements in between, converged stress solutions were obtained for a mesh with only 14 elements (Figure 6.5).

Figure 6.5 also shows the bulging pattern of ventricular deformation in

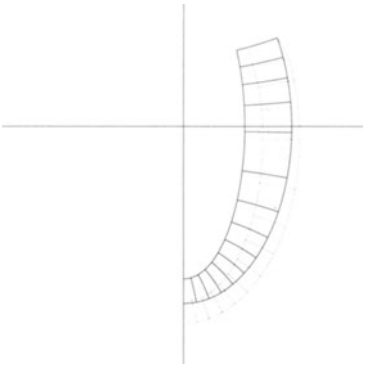

FIGURE 6.5. Fourteen-element prolate spheroidal model of the canine left ventricle. The unloaded reference shape (solid lines) and muscle-fiber angle distribution were the same as for the one-element model in Figure 6.2. The dotted lines show the deformed profile for a ventricular pressure of 2 kPa (15 mm Hg) with the base constrained from displacing at the epicardial node to simulate the effects of the stiff mitral valve ring.

contrast with the one-element model (Figure 6.2). The principal epicardial extensions near the equatorial region for ventricular pressures of 0 to 2.0 kPa are shown by the dashed line in Figure 6.3. The comparison with the one-element model and the experimental measurements shows that the effect of the basal constraint was significant and the agreement with the experimental data was excellent. Not only were the predicted principal directions of the major stretch within one standard error of the measurements, but they displayed the same variation with load as the measured means (Figure 6.4, dashed line). Consequently, the torsional displacements of the model at the midventricle were almost identical to those measured in the dog heart (4.4° compared with 4.1° for a 75% volume inflation).

The longitudinal distribution of fiber stress midway through the wall thickness of the 14-element prolate spheroidal model is shown in Figure 6.6 for a ventricular pressure of 1 kPa (7.5 mm Hg). The reasonably continuous stress distribution suggests that the convergence for this solution is good. The stresses appear to change most rapidly at the apex owing to the rapid changes of curvature there. However, the real behavior in this region may be different because the assumption that the muscle fibers lie in the plane of the endocardial and epicardial surfaces is probably not valid near the apical infundibulum [71]. Although this model provides a converged solution for base-apex stress distributions, the longitudinal variation in wall thickness and transmural fiber angle distribution of the left ventricle should also be included.

The prolate spheroidal nodal coordinates and fiber angle values of the 14-element axisymmetric mesh shown in Figure 6.7 were fitted to the anatom-

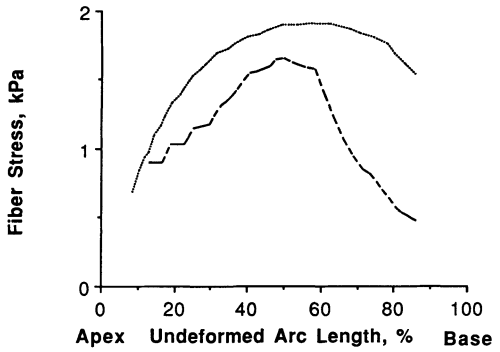


FIGURE 6.6. Longitudinal distribution of fiber stress midway through the wall thickness at a ventricular pressure of 1 kPa (7.5 mm Hg). The dotted line shows the solution for the fourteen-element prolate spheroidal model, and the dashed line corresponds to the axisymmetric model shown in Figure 6.7. Note that the stresses in the latter model were significantly lower in the basal region, and had a peak slightly nearer the apex.

ical measurements of Nielsen and coworkers at a section 36° from the anterior border of the left ventricular free wall along the same meridian on which the experimental measurements were made. The element spacing is the same as in the previous confocal prolate spheroidal mesh. Figure 6.6 shows the longitudinal distribution of fiber stress at midwall predicted by this model for a ventricular pressure of 1.0 kPa. This figure also shows that these midwall stresses were significantly lower in the basal region than those in the more idealized prolate spheroidal geometry. The deformed model shape at a load of 2.0 kPa is also shown in Figure 6.7. Again, a bulging deformation is produced by inflation with very little displacement near the fixed base.

Figure 6.8 shows the profiles from base to apex of principal epicardial strains predicted by the axisymmetric finite element model in comparison with experimental measurements at a low, medium, and high end-diastolic volume. The strains all rise from the base to a peak at about 50% along the arc length from the apex, and then again toward the apex. The model predictions appear to agree quite well with the experimental data at the basal and midventricular sites but are too low near the apex where the epicardial solutions may not be fully converged. The epicardial shear strains were negative at all volumes and fairly uniform throughout the longitude, except near the apex where they decreased rapidly to approximately zero.

The model predictions may well be improved by employing a cross-section that is thinner in the apical region. In fact, the circumferential component of epicardial strain predicted by the 14-element model shown in Figure 6.5 increased from the base to a peak much nearer the apex and

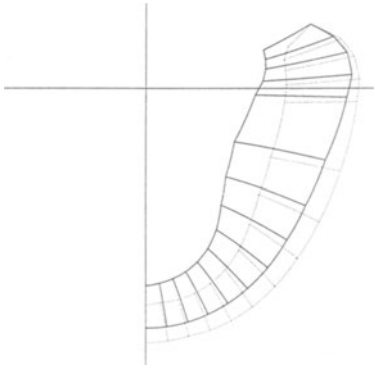

FIGURE 6.7. Fourteen-element axisymmetric model fitted by least squares to anatomical measurements from a cross-section of the anterior free wall of the canine left ventricle [56]. In the unloaded reference state (solid lines), ventricular cavity volume was 37 ml and wall volume was 125 ml. Within each element fiber angle varied linearly both in the transmural and longitudinal directions. Epicardial fiber angles varied between −43° at the base and −53° at the apex. On the endocardium, fiber angle increased continuously from 82° at the base to 97° at the apex. The dotted lines show the deformed profile for a diastolic ventricular pressure of 2 kPa (15 mm Hg) with the base constrained.

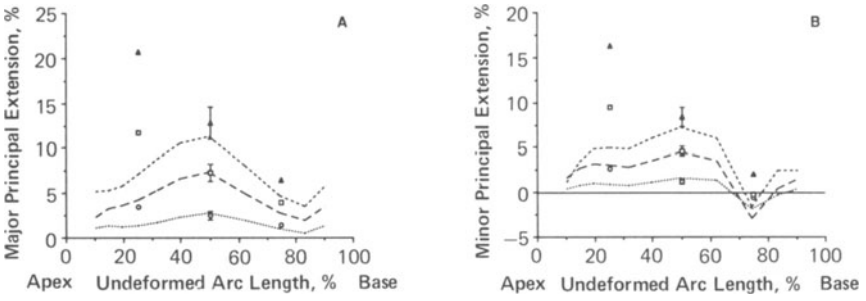


FIGURE 6.8. Longitudinal profiles of principal epicardial extensions at low, medium, and high left ventricular diastolic volumes. The lines show the predictions of the axisymmetric model shown in Figure 6.7 for increases in cavity volume of 15% (dotted line), 45% (long-dashed line), and 75% (short-dashed line). The symbols show the experimental measurements at three epicardial locations on the anterior free wall for the same three volume loads (circles, squares, and triangles, respectively). (A) Major epicardial percent extension. (B) Minor epicardial percent extension.

agreed closely with experimental results, especially at the apical and mid-ventricular sites. In that model, however, the longitudinal strain decreased slightly from base to apex in contrast to experimental observations.

A further extension to a fully three-dimensional finite element geometry is also needed. Although the regional measurements available for validating such a model remain scant, three-dimensional data will clearly be needed to understand the effects of such important factors as left and right ventricular interactions. On the other hand, since the axisymmetric model presented here is able to simulate many of the properties of the passive left ventricle, at least in significant regions of the free wall, it may be a useful starting point for a model of the active contraction of the ventricular myocardium through the cardiac cycle.

*Acknowledgements:* We are grateful to Dr. Peter J. Hunter, who initiated the development of our finite element models of the heart and has continued to extend the scope of the methods over the past 10 years. We would also like to thank Professor Y-C Fung, Dr. Poul M.F. Nielsen, and Dr. Lewis K. Waldman for their valuable advice and contributions to this work. This research was supported by PHS grant HL41603 and J.M. Guccione was supported by PHS Predoctoral Training Grant HL07089. This support is gratefully acknowledged.

## REFERENCES

[1] H. Abe and T. Nakamura. Finite deformation model for the mechanical behavior of left ventricular wall muscles. *Math. Modeling*, 3:143–152, 1982.

[2] N.R. Alpert. *Cardiac Hypertrophy.* Academic Press, New York, 1971.

[3] J.H. Argyris and S. Kelsey. *Energy Theorems and Structural Analysis.* Butterworths, London, 1960.

[4] T. Arts and R.S. Reneman. Dynamics of left ventricular wall and mitral valve mechanics—A model study. *J. Biomech.*, 22:261–271, 1989.

[5] T. Arts, R.S. Reneman, and P.C. Veenstra. Epicardial deformation and left ventricular wall mechanics during ejection in the dog. *Am. J. Physiol.*, 243:H379–H390, 1982.

[6] T. Arts, R.S. Reneman, and P.C. Veenstra. A model of the mechanics of the left ventricle. *Ann. Biomed. Eng.*, 7:299–318, 1979.

[7] D.A. Bergel and P.J. Hunter. The mechanics of the heart. In D.R. Gross, N.H.C. Hwang and D.J. Patel, editors, *Quantitative Cardio-*

*vascular Studies*, pages 151–213, University Park Press, Baltimore, 1979.

[8] R. Beyar and S. Sideman. The dynamic twisting of the left ventricle: A computer study. *Ann. Biomed. Eng.*, 14:547–562, 1986.

[9] D.K. Bogen, S.A. Rabinowitz, A. Needleman, T.A. McMahon, and W.H. Abelmann. An analysis of the mechanical disadvantage of myocardial infarction in the canine left ventricle. *Circ. Res.*, 47:728–741, 1980.

[10] T.K. Borg, W.F. Ranson, and F.A. Moslehy. Structural basis of ventricular stiffness. *Lab. Invest.*, 44:49–54, 1981.

[11] R.S. Chadwick. Mechanics of the left ventricle. *J. Biophys.*, 39:279–288, 1982.

[12] C.J. Chen, B.M. Kwak, K. Rim, and H.L. Falsetti. A model for an active left ventricle deformation—Formulation of a nonlinear quasi-steady finite element analysis for orthotropic, three-dimensional myocardium. *International Conference on Finite Elements in Biomechanics*, 2:640–655, 1980.

[13] R.D. Cook. *Concepts and Applications of Finite Element Analysis.* John Wiley & Sons, New York, 1981.

[14] L.L. Demer and F.C.P. Yin. Passive biaxial mechanical properties of isolated canine myocardium. *J. Physiol. Lond.*, 339:615–630, 1983.

[15] H. Demiray. Stresses in ventricular wall. *ASME J. Appl. Mech.*, 43: 194–197, 1976.

[16] H.L. Falsetti, R.E. Mates, C. Grant, D.G. Green, and I.L. Bunnell. Left ventricular wall stress calculated from one-plane cineangiography. *Circ. Res.*, 26:71–83, 1970.

[17] T.S. Feit. Diastolic pressure-volume relations and distribution of pressure and fiber extension across the wall of a model left ventricle. *J. Biophys.*, 28:143–166, 1979.

[18] M.P. Feneley, C.O. Olsen, D.D. Glower, and J.S. Rankin. Effect of acutely increased right ventricular afterload on work output from the left ventricle in conscious dogs. *Circ. Res.*, 65:135–145, 1989.

[19] Y.C. Fung. *Biodynamics: Circulation.* Springer-Verlag, New York, 1984.

[20] D.N. Ghista and M.S. Hamid. Finite element analysis of the human left ventricle whose irregular shape is developed from single plane cineangiocardiogram. *Comp. Prog. Biomed.*, 7:219–231, 1977.

[21] D.N. Ghista and H. Sandler. An analytic elastic-viscoelastic model for the shape and the forces in the left ventricle. *J. Biomech.*, 2:35–47, 1969.

[22] S.A. Glantz, G.A. Misbach, W.Y. Moores, et al. The pericardium substantially affects the left ventricular diastolic pressure-volume relationship in the dog. *Circ. Res.*, 42:433–441, 1978.

[23] P. Gould, D. Ghista, L. Brombolich, and I. Mirsky. In vivo stresses in the human left ventricular wall: Analysis accounting for the irregular 3-dimensional geometry and comparison with idealised geometry analysis. *J. Biomech.*, 5:521–539, 1972.

[24] J.M. Guccione Jr., A.D. McCulloch, and L.K. Waldman. Passive material properties of intact ventricular myocardium determined from a cylindrical model. *ASME J. Biomech. Eng.*, 113, 1991 (in press).

[25] M.S. Hamid, H.N. Sabbah, and P.D. Stein. Determination of left ventricular wall stress during isovolumic contraction using incompressible finite elements. *Comp. Struc.*, 24:589–594, 1986.

[26] D.E. Hansen, G.E. Sarris, M.A. Niczyporuk, G.C. Derby, P.D. Cahill, and D.C. Miller. Physiologic role of the mitral apparatus in left ventricular regional mechanics, contraction synergy, and global systolic performance. *J. Thorac. Cardiovasc. Surg.*, 97:521–533, 1989.

[27] R.M. Heethaar, Y.C. Pao, and E.L. Ritman. Computer aspects of three-dimensional finite element analysis of stresses and stains in the intact heart. *Comp. Biomed. Res.*, 10:271–285, 1977.

[28] A. Horowitz, I. Sheinman, and Y. Lanir. Nonlinear incompressible finite element for simulating loading of cardiac tissue—Part II: Three dimensional formulation for thick ventricular wall segments. *ASME J. Biomech. Eng.*, 110:62–68, 1988.

[29] R.M. Huisman, G. Elzinga, N. Westerhof, and P. Sipkema. Measurement of left ventricular wall stress. *Cardiovasc. Res.*, 14:142–153, 1980.

[30] J.D. Humphrey and F.C.P. Yin. Biaxial mechanical behavior of excised epicardium. *ASME J. Biomech. Eng.*, 110:349–351, 1988.

[31] P.J. Hunter, A.D. McCulloch, P.M.F. Nielsen, and B.H. Smaill. A finite element model of passive ventricular mechanics. In R.L. Spilker and B.R. Simon, editors, *Computational Methods in Bioengineering*, pages 387–397, ASME, New York, 1988.

[32] P.J. Hunter and B.H. Smaill. The analysis of cardiac function: A continuum approach. *Prog. Biophys. Molec. Biol.*, 52:101–164, 1988.

[33] N.B. Ingels Jr., D.E. Hansen, G.T. Daughters II, E.B. Stinson, E.L. Alderman, and D.C. Miller. Relation between longitudinal, circumferential, and oblique shortening and torsional deformation in the left ventricle of the transplanted human heart. *Circ. Res.*, 64:915–927, 1989.

[34] K.M. Jan. Distribution of myocardial stress and its influence on coronary blood flow. *J. Biomech.*, 18:815–820, 1985.

[35] R.F. Janz. Estimation of local myocardial stess. *Am. J. Physiol.*, 242:H875–H881, 1982.

[36] R.F. Janz and A.F. Grimm. Deformation of the diastolic left ventricle. I. nonlinear elastic effects. *Biophys. J.*, 13:689–704, 1973.

[37] R.F. Janz and A.F. Grimm. Finite element model for the mechanical behavior of the left ventricle. *Circ. Res.*, 30:244–252, 1972.

[38] R.F. Janz, B.R. Kubert, and T.F. Moriarty. Deformation of the diastolic left ventricle. II. Nonlinear geometric effects. *J. Biomech.*, 7:509–516, 1974.

[39] R.F. Janz, S. Ozpetek, L.E. Ginzton, and M.M. Laks. Regional stress in a noncircular cylinder. *Biophys. J.*, 55:173–182, 1989.

[40] R.F. Janz and R.J. Waldron. Predicted effect of chronic apical aneurysms on the passive stiffness of the human left ventricle. *Circ. Res.*, 42:255–263, 1978.

[41] Y. Kong, J.J. Morris Jr., and H.D. McIntosh. Assessment of regional myocardial performance from biplane coronary cineangiograms. *Am. J. Cardiol.*, 27:529–537, 1971.

[42] P. Le Tallec. Compatibility condition and existence results in discrete finite incompressible elasticity. *Comp. Meth. Appl. Math. Eng.*, 27:239–259, 1981.

[43] M.C. Lee, Y.C. Fung, R. Shabetai, and M.M. LeWinter. Biaxial mechanical properties of human pericardium and canine comparisons. *Am. J. Physiol.*, 253:H75–82, 1987.

[44] W.Y.W. Lew. Influence of ischemic zone size on nonischemic area function in the canine left ventricle. *Am. J. Physiol.*, 252:H990–H997, 1987.

[45] W.Y.W. Lew and M.M. LeWinter. Regional comparison of midwall segment and area shortening in canine left ventricle. *Circ. Res.*, 58:678–691, 1986.

[46] M.M. LeWinter, R.S. Kent, J.M. Kroener, T.E. Carew, and J.W. Covell. Regional difference in myocardial performance in the left ventricle. *Circ. Res.*, 37:191–199, 1975.

[47] A.D. McCulloch. *Deformation and Stress in the Passive Heart.* Ph.D. thesis, University of Auckland, New Zealand, 1986.

[48] A.D. McCulloch, B.H. Smaill, and P.J. Hunter. Regional left ventricular epicardial deformation in the passive dog heart. *Circ. Res.*, 64:721–733, 1989.

[49] C.D. Meier, A.A. Bove, W.P. Santamore, and P.R. Lynch. Contractile function in the canine right ventricle. *Am. J. Physiol.*, 39:H794–804, 1980.

[50] R.J. Melosh and P.V. Marcal. An energy basis for mesh refinement of strectural continua. *Int. J. Num. Meth. Eng.*, 11:1083–1091, 1977.

[51] I. Mirsky. Effects of anisotropy and nonhomogeneity on left ventricular stresses in the intact heart. *Bull. Math. Biophys.*, 32:197–213, 1970.

[52] I. Mirsky. Left ventricular stresses in the intact human heart. *Biophys. J.*, 9:189–208, 1969.

[53] I. Mirsky. Ventricular and arterial wall stresses based on large deformation analyses. *Biophys. J.*, 13:1141–1159, 1973.

[54] T.F. Moriarty. Law of Laplace: Its limitations as a relation for diastolic pressure, volume or wall stress of the left ventricle. *Circ. Res.*, 46:321–331, 1980.

[55] A. Needleman, S.A. Rabinowitz, D.K. Bogen, and T.A. McMahon. A finite element model of infarcted left ventricle. *J. Biomech.*, 16:45–58, 1983.

[56] P.M.F. Nielsen, I.J. LeGrice, B.H. Smaill, and P.J. Hunter. A mathematical model of the geometry and fibrous structure of the heart. *Am. J. Physiol.*, 1991, (in press).

[57] J. Ohayon and R.S. Chadwick. Theoretical analysis of the effects of a radial activation wave and twisting motion on the mechanics of the left ventricle. *Biorheology*, 25:435–447, 1988b.

[58] J. Ohayon and R.S. Chadwick. Theoretical analysis of the effects of a radial activation wave and twisting motion on the mechanics of the left ventricle. *Biophys. J.*, 54:1077–1088, 1988a.

[59] J.H. Omens and Y.C. Fung. Residual strain in rat left ventricle. *Circ. Res.*, 66:37–45, 1990.

[60] C.S. Panda and R. Natarajan. Finite method of stress analysis in the human left ventricular layered wall structure. *Med. Biol. Eng. Comp.*, 15:67–71, 1977.

[61] Y.C. Pao, E.L. Ritman, and E.H. Wood. Finite-element analysis of left ventricular myocardial stresses. *J. Biomech.*, 7:469–477, 1974.

[62] Y.C. Pao, R.A. Robb, and E.L. Ritman. Plane-strain finite-element analysis of reconstituted diastolic left ventricular cross section. *Ann. Biomed. Eng.*, 4:232–249, 1976.

[63] M. Perl, A. Horowitz, and S. Sideman. Comprehensive model for the simulation of left ventricle mechanics. Part I. Model description and simulation procedure. *Med. Biol. Eng. Comp.*, 24:145–149, 1986.

[64] J.G. Pinto and Y.C. Fung. Mechanical properties of the heart muscle in the passive state. *J. Biomech.*, 6:597–616, 1973.

[65] E.L. Ritman, R.M. Heethaar, R.A. Robb, and Y.C. Pao. Finite element analysis of myocardial diastolic stress and strain relationships in the intact heart. *Eur. J. Cardiol.*, 7:105–119, 1978.

[66] T.F. Robinson, L. Cohen-Gould, and S.M. Factor. Skeletal framework of mammalian heart muscle: Arrangement of inter- and pericellular connective tissue structures. *Lab. Invest.*, 49:482–498, 1983.

[67] H. Sandler and H.T. Dodge. Left ventricular tension and stress in man. *Circ. Res.*, 13:91–104, 1963.

[68] S.J. Sarnoff, E. Braunwald, G.H. Welch Jr., R.B. Case, W.N. Stainsby, and R. Macruz. Hemodynamic determinants of oxygen consumption of the heart with special reference to the tension-time index. *Am. J. Physiol.*, 192:148–156, 1958.

[69] P.N. Shivakumar, C-S. Man, and S.W. Rabkin. Modelling of the heart and pericardium at end-diastole. *J. Biomech.*, 22:201–209, 1989.

[70] B.K. Slinker, Y. Goto, and M.M. LeWinter. Systolic direct ventricular interaction affects left ventricular contraction and relaxation in the intact dog circulation. *Circ. Res.*, 65:307–315, 1989.

[71] D.D. Streeter. Gross morphology and fiber geometry of the heart. In R.M. Berne, editor, *Handbook of Physiology*, pages 339–350, American Physiological Society, Bethesda, MD, 1979.

[72] D.D. Streeter Jr. and W.T. Hanna. Engineering mechanics for successive states in canine left ventricular myocardium: II. Fiber angle and sarcomere length. *Circ. Res.*, 33:656–664, 1973b.

[73] D.D. Streeter Jr. and W.T. Hanna. Engineering mechanics for successive states in canine left ventricular myocardium: I. Cavity and wall geometry. *Circ. Res.*, 33:639–655, 1973a.

[74] H.E.D.J. Ter Keurs, W.H. Rijnsburger, R. Van Heuningen, and M.J. Nagelsmit. Tension development and sarcomere length in rat cardiac trabeculae: Evidence of length-dependent activation. *Circ. Res.*, 46:703–71, 1980.

[75] P. Theroux, J. Ross Jr., D. Franklin, J.W. Covell, C.M. Bloor, and S. Sasayama. Regional myocardial function and dimensions early and late after myocardial infarction in the unanesthetized dog. *Circ. Res.*, 40:158–165, 1977.

[76] A. Tözeren. Static analysis of the left ventricle. *ASME J. Biomech. Eng.*, 105:39–46, 1983.

[77] D.J. Turcke and G.M. McNeice. Guidelines for selecting finite element grids based on an optimization study. *Comp. Struc.*, 4:499–519, 1974.

[78] M.J. Turner, R.W. Clough, H.C. Martin, and L.J. Topp. Stiffness and deflection analysis of complex structures. *J. Aero. Sci.*, 9:805–823, 1956.

[79] J.H.J.M. Van den Broek and J.J. Denier Van der Gon. A model study of isovolumic and nonisovolumic left ventricular contractions. *J. Biomech.*, 13:77–87, 1980.

[80] J.H.J.M. Van den Broek and M.H.L.M. Van den Broek. Application of an ellipsoidal heart model in studying left ventricular contractions. *J. Biomech.*, 13:493–503, 1980.

[81] D.L. Vawter. Poisson's ratio and incompressiblity. *ASME J. Biomech. Eng.*, 105:194–195, 1983.

[82] C.A. Vinsen, D.G. Gibson, and A.L. Yettram. Analysis of left ventricular behavior in diastole by means of finite element method. *Br. Heart. J.*, 41:60–67, 1979.

[83] R.P. Vito. The role of the pericardium in cardiac mechanics. *J. Biomech.*, 12:587–592, 1979.

[84] L.K. Waldman, Y.C. Fung, and J.W. Covell. Transmural myocardial deformation in the canine left ventricle: Normal in vivo three-dimensional finite strains. *Circ. Res.*, 57:152–163, 1985.

[85] L.K. Waldman, D. Nosan, F.J. Villarreal, and J.W. Covell. Relation between transmural deformation and local myofiber direction in canine left ventricle. *Circ. Res.*, 63:550–562, 1985.

[86] M.L. Walker, E.W. Hawthorne, and H. Sandler. Methods for assessing performance for the intact hypertrophied heart. In N.R. Alpert, editor, *Cardiac Hypertrophy*, pages 387–405, Academic Press, New York, 1971.

[87] A.Y.K. Wong and P.M. Rautaharju. Stress distribution within the left ventricular wall approximated as a thick ellipsoidal shell. *Am. Heart. J.*, 75:649–662, 1968.

[88] R.H. Woods. A few applications of a physical theorem to membranes in the human body in a state of tension. *J. Anat. Physiol.*, 26:362–270, 1892.

[89] A.L. Yettram, C.A. Vinson, and D.G. Gibson. Effect of myocardial fibre architecture on the behaviour of the human left ventricle in diastole. *J. Biomed. Eng.*, 5:321–328, 1983.

[90] F.C.P. Yin. Ventricular wall stress. *Circ. Res.*, 49:829–842, 1981.

[91] F.C.P. Yin, R.K. Strumpf, P.H. Chew, and S.L. Zeger. Quantification of the mechanical properities of noncontracting canine myocardium under simultaneous biaxial loading. *J. Biomech.*, 20:577–589, 1987.

[92] F.C.P. Yin, S. Zeger, R. Strumpf, L. Demer, P. Chew, and W.L. Maughan. Assessment of regional ventricular mechanics. In C. Taylor, E. Hinton, D. Owen, E. Orate, editors, *Numerical Methods for Nonlinear Problems*, Pineridge Press, Swansea, U.K., page 513, 1984.